*J. Fluid Mech.* (1979), *vol.* 91, *part* 1, *pp.* 93–110
*Printed in Great Britain*



# Steady streaming induced between oscillating cylinders

By P. W. DUCK† AND F. T. SMITH
Department of Mathematics, Imperial College, London

(Received 19 August 1976 and in revised form 21 August 1978)

The flow of an incompressible fluid contained between two infinitely long circular cylinders is considered when the inner cylinder performs small harmonic oscillations about the centre of the larger (fixed) cylinder. Numerical solutions are presented for the Navier–Stokes equations governing the steady-streaming component of the motion. Special attention is then paid to this flow when the Reynolds number of the steady streaming is large, and when the radius of the outer cylinder is much larger than that of the inner. Results obtained show an improved correlation with experimental results and indicate strongly that the finiteness of the domain is the major cause of the discrepancies between experiment and previous theoretical studies.

## 1. Introduction

Much attention has been given to the incompressible fluid flow produced between two aligned, infinitely long, circular cylinders when the inner cylinder performs small harmonic oscillations about the centre of the larger one. For definiteness, let us introduce the notation immediately. If the velocity of the inner cylinder is $U_0^* \cos \omega t^*$, then it is found convenient to use the following dimensionless parameters:

$$\left.\begin{aligned} \epsilon = U_0^*/\omega a, \quad M^2 = \omega a^2/\nu, \\ R = U_0^* a/\nu = \epsilon M^2, \quad R_s = U_0^{*2}/\omega\nu = \epsilon^2 M^2, \quad \alpha = b/a. \end{aligned}\right\} \tag{1.1}$$

Here $a$ and $b$ are the radii of the inner and outer cylinder respectively, and $\nu$ is the kinematic viscosity of the fluid. Throughout this paper, it is assumed that $\epsilon \ll 1$, i.e. the ratio of the amplitude of oscillation is small compared with the radius of the inner cylinder, and that the motion is laminar and two-dimensional.

Segel (1961) studied the allied problem where the larger cylinder oscillates about the centre of the smaller one, which is fixed, but restricted his discussion to situations for which $M \ll 1$. Holtsmark *et al.* (1954) considered a perturbation solution for $\epsilon \ll 1$ for an oscillating circular cylinder both in an unbounded fluid and also for the case where there is an outer container. Their results hold formally for $M = O(1)$ and $R \ll 1$. Skavlem & Tjøtta (1955) noted that the outer boundary conditions applied by Holtsmark *et al.* (1954) were not quite correct and repeated the analysis for the contained-fluid example. Later Wang (1968) used an inner–outer expansion method for the $R = O(1)$ regime for an oscillating cylinder in an unbounded fluid. Bertelsen, Svardal & Tjøtta (1973) obtained new theoretical and experimental results for the two-cylinder case for $M = O(1)$, and obtained good correlation between their two sets of results.

† Present address: Department of Aeronautical and Astronautical Engineering, Ohio State University, Columbus, Ohio 43210.

0022–1120/79/4166–5860 $02.00 

However, to date all theoretical work on the large-$R_s$ regime has been restricted to the problem of one cylinder oscillating in an infinite medium. Stuart (1963, 1966) and Riley (1965) treated the problem of a circular cylinder immersed in a fluctuating external flow (any enclosures then being assumed to be at infinity). The Stokes layer on the single cylinder has a steady secondary component which induces a steady streaming through the entire flow field, the character of which is determined by the magnitude of the steady-streaming Reynolds number $R_s$. Our eventual concern here is with the flow for large values of $R_s$, although we consider also small values (following Riley's (1967) approach) since most of the results are also applicable to the large-$R_s$ regime. For large $R_s$ the boundary layers emanating from the poles of the cylinder collide at the equator, giving rise to a free jet in the fluid; Smith & Duck (1977) consider the manner of the flow adjustment near the equator. Davidson & Riley (1972) observed experimentally that the jet then achieves approximately the Bickley (1937) similarity jet solution within about one diameter from the point of separation at the equator.

In an attempt to reduce the discrepancy between the experimental results of Bertelsen (1974) (for the two-cylinder problem) and previous theoretical work for the single-cylinder problem, Riley (1975) carried his calculations to an order higher in $R_s^{-1}$, using the Bickley jet solution to model the complete free jet. This last work is significant in that it showed that the $R_s$ effects do not resolve all the discrepancies, particularly at the edge of the Reynolds boundary layer, where Bertelsen's experiments (performed for $\alpha = 13{\cdot}03$ and $20{\cdot}67$, with $R_s = 400$ and 90 in turn) indicated a residual slip.

One is led, therefore, to consider the influence of large but finite values of $\alpha$. In an initial attempt (not reported here) made by the present authors to describe the influence of large values of $\alpha$, the conclusion was reached that the relative error in the one-cylinder approach is as large as $O(\alpha^{-\frac{1}{2}})$, which suggests that the $\alpha$ effects are indeed more important than the $R_s$ effects in practice. However, a referee kindly pointed out an inconsistency in that initial attempt. Accordingly, it was decided that the steady-streaming problem would best be solved for finite values of $\alpha$ and $R_s$, with a view to extracting from the results the trends of the flow solution as $\alpha$ and $R_s$ increase. The required numerical solutions (of the Navier–Stokes equations) and their trends are reported in § 4 below, and they strongly support the following separated flow model (the main points of which bear out the views and expectations of Prof. J. T. Stuart 1976–7, private communications) for large values of $\alpha$ and $R_s$. The asymptotic solution consists of an inviscid core region (the majority of the flow field), which has closed streamlines with constant vorticity (Batchelor 1956), and a closed boundary-layer structure, produced by the slip velocity of the core and in which the inner cylinder acts as a point source of momentum. Thus the induced jet from the inner cylinder expands into the boundary layer, which then hits the outer cylinder at its equator and passes some way along the outer cylinder. To avoid deceleration (and hence catastrophic separation; Stewartson 1970) near the pole, the boundary layer separates in a regular, triple-deck, fashion (Sychev 1972; Smith 1977) before reaching the pole and forms a free shear layer. This layer sweeps almost unaltered past the inner cylinder, thus giving rise to an effective slip at the edge of the thin boundary layer there, and finally completes the closed circuit by supplementing the original boundary layer. The results bear out (see § 5) our initial conclusion of a (sizable) $O(\alpha^{-\frac{1}{2}})$ correction when $\alpha$ is large (as well as supporting the referee's earlier objection) and show much improved corre-

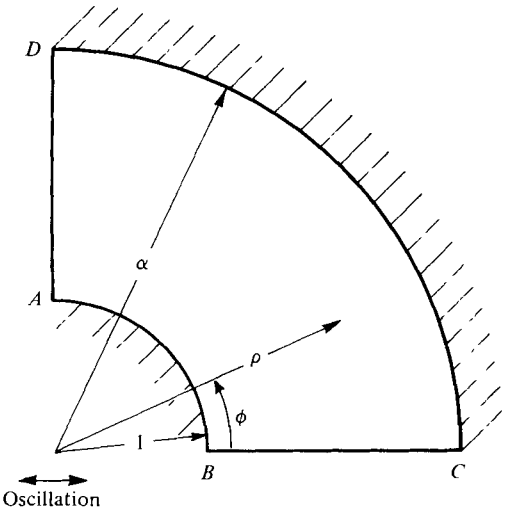


FIGURE 1. Definition sketch of the flow problem in the $\zeta$ plane.

lation (see figure 6 below) with Bertelsen's (1974) experiments. Although $\alpha^{-1}$ and $R_s^{-\frac{1}{2}}$ are comparable in the experiments, it is the fact that the large-$\alpha$ solution proceeds in powers of $\alpha^{-\frac{1}{2}}$ which makes the influence of the closed domain so marked.

Our major effort, then, is aimed at analysing the effects of the finiteness of the domain in practice. The problem is stated in § 2 below. A limiting situation is then studied in § 3, namely $1 \ll M \ll \epsilon^{-1}$ ($R_s \ll 1$), and numerical solutions are presented in § 4 for $O(1)$ values of $R_s$ (and $\alpha$). This leads into the large-$\alpha$ theory and comparisons of § 5. For a more detailed survey of the early work on these oscillating viscous flows, the reader is referred to Riley (1967).

## 2. Statement of the problem

Suppose that we take polar co-ordinates $(r, \theta)$ with origin at the centre of the outer (fixed) cylinder, in the $z$ plane, and that the position of the centre of the inner cylinder varies as $z = \epsilon a \cos \omega t^*$ ($\epsilon \ll 1$), where $t^*$ is dimensional time and $\omega$ the frequency of oscillation. The outer cylinder is described by $z = b e^{i\theta}$. We map the $z$ plane onto the $\zeta$ plane using a conformal transformation similar to that of Segel (1961):

$$\zeta = \frac{z - \epsilon a \cos \omega t^* - a\gamma}{a + \gamma \epsilon a \cos \omega t^* - z\gamma} = \rho e^{i\phi}, \tag{2.1}$$

where

$$\gamma = \frac{2\epsilon \cos \omega t^*}{\alpha^2 - 1 - \epsilon^2 \cos^2 \omega t^* + [(\alpha^2 - 1 - \epsilon^2 \cos^2 \omega t^*)^2 - 4\epsilon^2 \cos^2 \omega t^*]^{\frac{1}{2}}}. \tag{2.2}$$

This transformation maps the inner cylinder onto $\rho = 1$ and the outer onto

$$\rho = \alpha/(1 + \gamma\epsilon) = \alpha + O(\epsilon^2), \tag{2.3}$$

so to order $\epsilon^2$ the outer cylinder maps to a circle of radius $\alpha$ in the $\zeta$ plane (see figure 1).

If we non-dimensionalize (time with respect to $1/\omega$, distances with respect to $a$) and introduce a stream function $\psi$, the Navier–Stokes equations may be written in the form

$$J\frac{\partial}{\partial t}\left(\frac{\Delta\psi}{J}\right)+\frac{\epsilon}{\rho}\frac{\partial(\Delta\psi/J,\psi)}{\partial(\rho,\phi)}=\frac{1}{M^2}\Delta\left(\frac{\Delta\psi}{J}\right). \tag{2.4}$$

Here the Jacobian $J=J(\rho,\phi,t)$ is given by

$$\begin{aligned}J=\frac{1}{a^2}\left|\frac{dz}{d\zeta}\right|^2&=(1-\gamma^2)^2(1+2\rho\gamma\cos\phi+\rho^2\gamma^2)^{-2}\\&=1-\frac{4\rho\epsilon\cos t\cos\phi}{\alpha^2-1}+O(\epsilon^2)\end{aligned} \tag{2.5}$$

and

$$\Delta\psi=\frac{\partial^2\psi}{\partial\rho^2}+\frac{1}{\rho}\frac{\partial\psi}{\partial\rho}+\frac{1}{\rho^2}\frac{\partial^2\psi}{\partial\phi^2}. \tag{2.6}$$

The boundary conditions are as follows:

$$\partial\psi/\partial\phi=\partial\psi/\partial\rho=0\quad\text{on}\quad\rho=\alpha+O(\epsilon^2), \tag{2.7a,b}$$

$$\left.\begin{aligned}\frac{\partial\psi}{\partial\phi}&=-\cos\phi\sin t+\frac{\epsilon\sin 2t\cos 2\phi}{\alpha^2-1}+O(\epsilon^2) &(2.8a)\\ \frac{\partial\psi}{\partial\rho}&=-\sin\phi\sin t+\frac{\epsilon\sin 2t\sin 2\phi}{\alpha^2-1}+O(\epsilon^2) &(2.8b)\end{aligned}\right\}\quad\text{on}\quad\rho=1.$$

The basic task, then, is to solve (2.4)–(2.8), which we now attempt for small values of $\epsilon$. We consider two particular regimes determined by the order of the non-dimensional parameter $R_s$.

## 3. Small steady-streaming Reynolds number $R_s$

This case is considered in detail because, although we shall eventually be concerned (in §§ 4 and 5) with $O(1)$ or large values of $R_s$, most of the results here are directly applicable in §§ 4 and 5 below. We expand the stream function in the following way:

$$\psi(\mathbf{x},t,M,\epsilon)=\psi_0(\mathbf{x},t,M)+\epsilon[\psi_1^{(u)}(\mathbf{x},t,M)+\psi_1^{(s)}(\mathbf{x},M)]+O(\epsilon^2). \tag{3.1}$$

Then the equations for the $\psi_i$ are

$$\partial(\Delta\psi_0)/\partial t=M^{-2}\Delta\Delta\psi_0, \tag{3.2}$$

$$\begin{aligned}\frac{\partial}{\partial t}(\Delta\psi_1^{(u)})-\frac{1}{M^2}\Delta\Delta\psi_1^{(u)}=-\Big\{&\frac{1}{\rho}\frac{\partial(\Delta\psi_0,\psi_0)}{\partial(\rho,\phi)}-\frac{4\rho\Delta\psi_0\sin t\cos\phi}{\alpha^2-1}\\&-\frac{1}{M^2}\Delta\left(\frac{4\rho\cos t\cos\phi\,\Delta\psi_0}{\alpha^2-1}\right)\Big\}^{(u)},\end{aligned} \tag{3.3}$$

$$\begin{aligned}\frac{1}{M^2}\Delta\Delta\psi_1^{(s)}=\Big\{&\frac{1}{\rho}\frac{\partial(\Delta\psi_0,\psi_0)}{\partial(\rho,\phi)}-\frac{4\rho\,\Delta\psi_0\sin t\cos\phi}{\alpha^2-1}\\&-\frac{1}{M^2}\Delta\left(\frac{4\rho\cos t\cos\phi\,\Delta\psi_0}{\alpha^2-1}\right)\Big\}^{(s)},\end{aligned} \tag{3.4}$$

where superscripts $(s)$ and $(u)$ denote steady and unsteady components respectively. The boundary conditions for $\psi_0$ are

$$\partial\psi_0/\partial\phi = \partial\psi_0/\partial\rho = 0 \quad \text{on} \quad \rho = \alpha, \tag{3.5a,b}$$

$$\partial\psi_0/\partial\phi = -\cos\phi\sin t, \quad \partial\psi_0/\partial\rho = -\sin\phi\sin t \quad \text{on} \quad \rho = 1. \tag{3.6a,b}$$

If we now let $M$ become large and expand $\psi_0$ in the form

$$\psi_0(\mathbf{x}, t, M) = \psi_{00}(\mathbf{x}, t) + M^{-1}\psi_{01}(\mathbf{x}, t) + O(M^{-2}), \tag{3.7}$$

then $\psi_{00}$ satisfies

$$\partial(\Delta\psi_{00})/\partial t = 0. \tag{3.8}$$

Because of the inviscid governing equation, the boundary conditions (3.5$b$) and (3.6$b$) are relaxed, so

$$\psi_{00} = \frac{\sin t\sin\phi}{\alpha^2-1}\left(\rho - \frac{\alpha^2}{\rho}\right). \tag{3.9}$$

In order to satisfy the slip conditions (3.5$b$) and (3.6$b$) there must be an inner boundary layer (the Stokes shear-wave layer). From standard boundary-layer arguments, this inner layer is of thickness $O(M^{-1})$ and we rescale $\psi$ and $\rho$ as follows:

$$\eta = M(\rho-1)/2^{\frac{1}{2}}, \quad \Psi = \frac{M}{2^{\frac{1}{2}}}\left[\psi + \rho\sin\phi\sin t - \frac{\epsilon\rho^2\sin 2t\sin 2\phi}{2(\alpha^2-1)}\right] \quad \text{for } \rho \sim 1.$$

$$\tilde{\eta} = M(\alpha-\rho)/2^{\frac{1}{2}}, \quad \tilde{\Psi} = M\psi/2^{\frac{1}{2}} \quad \text{for} \quad \rho \sim \alpha.$$

We then expand $\Psi(\eta, \phi, t, M, \epsilon)$ as

$$\Psi = \Psi_{00}(\eta,\phi,t) + M^{-1}\Psi_{01}(\eta,\phi,t) + O(M^{-2}) + \epsilon[\Psi_{10}^{(u)}(\eta,\phi,t) + \Psi_{10}^{(s)}(\eta,\phi) + O(M^{-2})] + O(\epsilon^2), \tag{3.10}$$

and similarly for $\tilde{\Psi}(\tilde{\eta}, \phi, t, M, \epsilon)$. Writing

$$\Psi_{00} = (2i)^{-1}\sin\phi[X_{00}(\eta)\,e^{it} - \bar{X}_{00}(\eta)\,e^{-it}] \tag{3.11}$$

(a bar denoting a complex conjugate), substituting into (3.2) and equating $O(M)$ terms gives

$$X_{00}(\eta) = \alpha^2\left(\frac{1-i}{\alpha^2-1}\right)\{\exp[-(1+i)\eta] - 1\} + \frac{2\alpha^2\eta}{\alpha^2-1}. \tag{3.12}$$

The condition at $\eta = \infty$ is obtained from $[\partial\psi_{00}/\partial\rho]_{\rho=1}$. Similarly

$$\tilde{X}_{00}(\tilde{\eta}) = \left(\frac{1-i}{\alpha^2-1}\right)\{1 - \exp[-(1+i)\tilde{\eta}]\} - \frac{2\tilde{\eta}}{\alpha^2-1}. \tag{3.13}$$

The term $\psi_{01}$ gives a correction to the inviscid flow and, omitting the details, we find that

$$\psi_{01} = \frac{2\alpha}{(\alpha^2-1)(1-\alpha)}\sin\phi\sin(t-\tfrac{1}{4}\pi)\left[\frac{1-\alpha+\alpha^2}{\rho} - \rho\right]. \tag{3.14}$$

Writing

$$\Psi_{01} = (2i)^{-1}\sin\phi[X_{01}(\eta)\,e^{it} - \bar{X}_{01}(\eta)\,e^{-it}], \tag{3.15}$$

the inner solution near $\rho = 1$ that matches with (3.14) is found to be

$$X_{01}(\eta) = \frac{i\alpha(\alpha^2-\alpha+4)}{2^{\frac{1}{2}}(\alpha^2-1)(1-\alpha)}\{\exp[-(1+i)\eta] - 1\} - \frac{2^{\frac{1}{2}}\alpha(1-i)(2-\alpha+\alpha^2)\eta}{(\alpha^2-1)(1-\alpha)} - \frac{\alpha^2}{2^{\frac{1}{2}}(\alpha^2-1)}\{2\eta^2 + (1-i)\eta\exp[-(1+i)\eta]\}. \tag{3.16}$$

Similarly

$$\bar{X}_{01}(\tilde{\eta}) = \frac{i(5\alpha^2-3\alpha+2)}{2^{\frac{1}{2}}\alpha(\alpha^2-1)(1-\alpha)}\{1-\exp[-(1+i)\tilde{\eta}]\}+\frac{2^{\frac{1}{2}}(1-i)(1-\alpha+2\alpha^2)\tilde{\eta}}{\alpha(\alpha^2-1)(1-\alpha)}$$
$$-\frac{1}{2^{\frac{1}{2}}(\alpha^2-1)}\{2i\tilde{\eta}^2+(1-i)\tilde{\eta}\exp[-(1+i)\tilde{\eta}]\}. \quad (3.17)$$

In principle the process of determining the $\psi_{0i}$, $\Psi_{0i}$ and $\tilde{\Psi}_{0i}$ may be continued indefinitely.

Consider next the $O(\epsilon)$ terms. We split these into two components, one unsteady, the other steady, the governing equations being (3.3) and (3.4) respectively. The boundary conditions for $\psi_1$ are

$$\partial\psi_1/\partial\phi = \partial\psi_1/\partial\rho = 0 \quad \text{on} \quad \rho = \alpha, \quad (3.18a,b)$$

$$\left.\begin{aligned}\partial\psi_1/\partial\phi &= \sin 2t\cos 2\phi/(\alpha^2-1) \quad (3.19a)\\ \partial\psi_1/\partial\rho &= \sin 2t\sin 2\phi/(\alpha^2-1) \quad (3.19b)\end{aligned}\right\} \quad \text{on} \quad \rho = 1.$$

If we again expand in inverse powers of $M$, for example

$$\psi_1^{(u)} = \psi_{10}^{(u)} + M^{-1}\psi_{11}^{(u)} + O(M^{-2}), \quad (3.20)$$

we find

$$\partial(\Delta\psi_{10}^{(u)})/\partial t = 0. \quad (3.21)$$

Then using (3.18$a$) and (3.19$a$), whilst relaxing (3.18$b$) and (3.19$b$), we obtain

$$\psi_{10}^{(u)} = \frac{-1}{2(\alpha^2-1)^2(1+\alpha^2)}\left(\rho^2-\frac{\alpha^4}{\rho^2}\right)\sin 2\phi\sin 2t. \quad (3.22)$$

Again a Stokes layer is assumed in order that (3.18$b$) and (3.19$b$) may be satisfied. We write

$$\Psi_{10}^{(u)} = (2i)^{-1}[X_{10}^{(u)}(\eta)\,e^{2it} - \bar{X}_{10}^{(u)}\,e^{-2it}]\sin 2\phi \quad (3.23)$$

(and similarly for $\tilde{\Psi}_{10}^{(u)}$) and find, using (3.3) and taking terms $O(M)$, that

$$X_{10}^{(u)}(\eta) = \frac{\alpha^4(1-i)}{2^{\frac{3}{2}}(\alpha^4-1)}\{1-\exp[-2^{\frac{1}{2}}(1+i)\eta]\}\frac{(3+\alpha^2)}{(\alpha^2-1)}$$
$$-\frac{\alpha^4}{(\alpha^2-1)^2}\eta\exp[-(1+i)\eta]-\frac{2\alpha^4\eta}{(\alpha^2-1)^2(1+\alpha^2)}. \quad (3.24)$$

Similarly

$$\bar{X}_{10}^{(u)}(\tilde{\eta}) = \frac{\alpha(1-i)}{2\sqrt{2(\alpha^4-1)}}\{\exp[-2^{\frac{1}{2}}(1+i)\tilde{\eta}]-1\}\frac{(3+\alpha^2)}{(\alpha^2-1)}$$
$$+\frac{\alpha}{(\alpha^2-1)^2}\tilde{\eta}\exp[-(1+i)\tilde{\eta}]+\frac{2\alpha\tilde{\eta}}{(\alpha^2-1)^2(1+\alpha^2)}. \quad (3.25)$$

If $\Psi_{10}^{(s)} = X_{10}^{(s)}(\eta)\sin 2\phi$, the problem for $X_{10}^{(s)}(\eta)$ may be stated in the form

$$X_{10\eta}^{(s)}(0) = X_{10}^{(s)}(0) = 0, \quad X_{10\eta}^{(s)}(\infty) \text{ finite}, \quad (3.26)$$

where the governing equation for $\Psi_{10}^{(s)}$ is obtained from (3.4). The solution for $X_{10}^{(s)}$ is found to be given by

$$X_{10}^{(s)}(\eta) = \frac{3\alpha^4}{2(\alpha^2-1)^2}\eta\frac{-\alpha^2(13\alpha^2+8)}{4(\alpha^2-1)^2}+\frac{\alpha^4}{4(\alpha^2-1)^2}e^{-2\eta}$$
$$+\frac{\alpha^2(3\alpha^2+2)}{(\alpha^2-1)^2}e^{-\eta}\cos\eta+\frac{2\alpha^2(\alpha^2+1)}{(\alpha^2-1)^2}e^{-\eta}\sin\eta+\frac{\alpha^4}{(\alpha^2-1)^2}\eta e^{-\eta}\sin\eta. \quad (3.27)$$

Similarly $\tilde{X}_{10}^{(s)}(\tilde{\eta})$ is given by

$$\tilde{X}_{10}^{(s)}(\tilde{\eta}) = -\frac{3}{2\alpha(\alpha^2-1)^2}\tilde{\eta} + \frac{13+8\alpha^2}{4\alpha(\alpha^2-1)^2} - \frac{1}{4\alpha(\alpha^2-1)^2}e^{-2\tilde{\eta}} - \frac{(2\alpha^2+3)}{\alpha(\alpha^2-1)^2}e^{-\tilde{\eta}}\cos\eta - \frac{2(\alpha^2+1)}{\alpha(\alpha^2-1)^2}e^{-\tilde{\eta}}\sin\tilde{\eta} - \frac{1}{\alpha(\alpha^2-1)^2}\tilde{\eta}\,e^{-\tilde{\eta}}\sin\tilde{\eta}. \quad (3.28)$$

We note that the Stokes layer near $\rho = 1$ produces a slip given by

$$\frac{\partial\psi_{10}^{(s)}}{\partial\rho} = \frac{3\alpha^4}{2(\alpha^2-1)^2}\sin 2\phi, \quad (3.29)$$

whilst the Stokes layer near $\rho = \alpha$ produces a slip given by

$$\frac{\partial\psi_{10}^{(s)}}{\partial\rho} = \frac{3}{2\alpha(\alpha^2-1)^2}\sin 2\phi. \quad (3.30)$$

The two other boundary conditions for $\psi_{10}^{(s)}$ are

$$\psi_{10}^{(s)}(1,\phi) = \psi_{10}^{(s)}(\alpha,\phi) = 0 \quad (3.31)$$

and the governing equation is found to be the biharmonic equation, i.e.

$$\Delta\Delta\psi_{10}^{(s)} = 0. \quad (3.32)$$

The solution is then given by

$$\psi_{10}^{(s)} = [3/4\alpha(\alpha^2-1)^4]\{(1+\alpha^4)\rho^4 - (1+\alpha^2)(2-\alpha^2+2\alpha^4)\rho^2 + (1+2\alpha^2+2\alpha^6+\alpha^8) - \alpha^2(1+\alpha^6)/\rho^2\}\sin 2\phi. \quad (3.33)$$

It can be shown that, in the limit $\alpha \to \infty$, $X_{00}(\eta)$, $X_{01}(\eta)$, $X_{10}^{(u)}(\eta)$ and $X_{10}^{(s)}(\eta)$ reduce to the forms stated by Riley (1967) and Wang (1968) for the one-cylinder problem. Similarly the work for $M = O(1)$ by Bertelsen *et al.* (1973) for two cylinders almost certainly reduces to (3.33) in the limit $M \to \infty$, although the algebra involved in verifying such a limiting process proves prohibitive.

## 4. Numerical solutions for $O(1)$ values of $R_s$ and $\alpha$

When $R_s$ is $O(1)$, expanding in the same way as in § 3, we find that $\psi_{00}$, $\psi_{01}$, $\Psi_{00}$, $\Psi_{01}$, $\tilde{\Psi}_{00}$, $\tilde{\Psi}_{01}$, $\psi_{10}^{(u)}$, $\Psi_{10}^{(u)}$ and $\tilde{\Psi}_{10}^{(u)}$ are unchanged. However it is found that the steady-streaming function $\psi_{10}^{(s)}$ is now given by

$$\frac{1}{R_s}\Delta\Delta\psi_{10}^{(s)} - \frac{1}{\rho}\frac{\partial(\Delta\psi_{10}^{(s)}, \psi_{10}^{(s)})}{\partial(\rho,\phi)} = 0, \quad (4.1)$$

i.e. $\psi_{10}^{(s)}$ is governed by the full steady Navier–Stokes equation and determines the steady streaming. This follows from consideration of the (steady) terms $O(\epsilon^3)$ in the basic equation (2.4), in much the same way as in Riley's (1967) analysis. The problem now [(4.1) with (3.29)–(3.31)] is identical with Stuart's (1966) and Riley's (1965) except for the presence of the outer cylinder and the slip velocity (3.30) on it.

Clearly, to compare with the experiments of Bertelsen (1974) it would be most desirable to obtain the asymptotic solution [to (4.1) with (3.29)–(3.31)] for large values of $R_s$ and $\alpha$. Our initial attempt (referred to in § 1) at such a solution proved unsuccessful, however, mainly because it was based on a predominantly jet-like model with

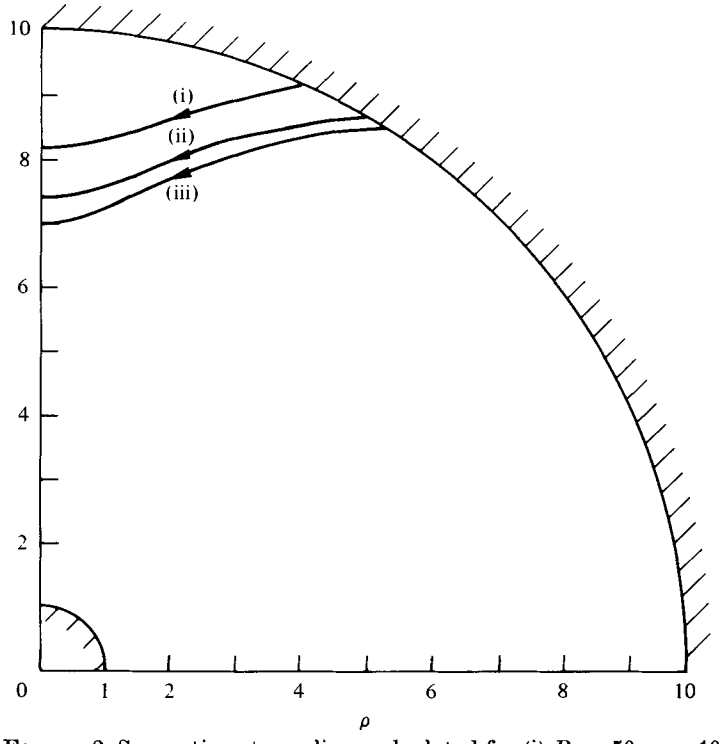


FIGURE 2. Separating streamlines calculated for (i) $R_s = 50$, $\alpha = 10$, (ii) $R_s = 70$, $\alpha = 10$ and (iii) $R_s = 90$, $\alpha = 10$.

attached flow. Therefore we undertook a numerical investigation of the Navier–Stokes problem (4.1) with (3.29)–(3.31) for a number of values of $\alpha$ and $R_s$.

The numerical method was an adaptation of that of McConalogue & Srivastava (1968). The stream function $\psi_{10}^{(s)}$ and the vorticity were expressed in sine series in $\phi$:

$$\psi_{10}^{(s)} = \sum_{m=1}^{\infty} \Psi_m(\rho) \sin 2m\phi, \quad \Delta\psi_{10}^{(s)} = \sum_{m=1}^{\infty} Z_m(\rho) \sin 2m\phi, \qquad (4.2), (4.3)$$

giving the infinite set of equations

$$Z_m'' + \frac{1}{\rho} Z_m' - \frac{4m^2}{\rho^2} Z_m = \frac{R_s}{\rho} \sum_{j=-\infty}^{\infty} [jZ_{m-j}' \Psi_j - (m-j) Z_{m-j} \Psi_j'] \qquad (4.4)$$

and

$$Z_m = \Psi_m'' + \frac{1}{\rho} \Psi_m' - \frac{4m^2}{\rho^2} \Psi_m \qquad (4.5)$$

from (4.1). Here we define

$$\Psi_m = -\Psi_{-m}, \quad Z_m = -Z_{-m}. \qquad (4.6)$$

The boundary conditions on (4.2) and (4.3) are [from (3.29)–(3.31)]

$$\left.\begin{aligned} \Psi_m(1) = \Psi_m(\alpha) = 0, \\ \Psi_m'(1) = \Psi_m'(\alpha) = 0 \quad (m \neq 1), \\ \Psi_1'(1) = 3\alpha^4/2(\alpha^2-1)^2, \quad \Psi_1'(\alpha) = 3/2\alpha(\alpha^2-1)^2. \end{aligned}\right\} \qquad (4.7)$$

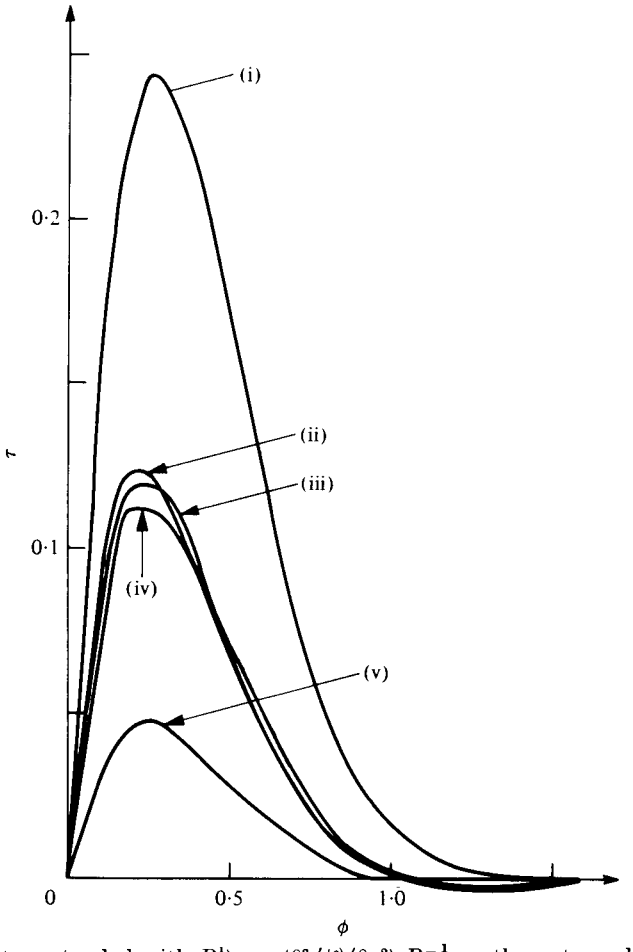


FIGURE 3. Shear stress (scaled with $R_s^{\frac{1}{2}}$) $\tau = (\partial^2\psi_{10}^{(s)}/\partial\rho^2)\, R_s^{-\frac{1}{2}}$ on the outer cylinder as a function of $\phi$ for (i) $R_s = 50$, $\alpha = 5$, (ii) $R_s = 90$, $\alpha = 10$, (iii) $R_s = 70$, $\alpha = 10$, (iv) $R_s = 50$, $\alpha = 10$, (v) $R_s = 50$, $\alpha = 20{\cdot}67$.

Next, each of the second-order equations (4.4) and (4.5) was broken down into two first-order equations, giving an infinite coupled set of first-order differential equations.

To solve this infinite set approximately, the system was first truncated and then discretized (using second-order differencing). The discrete system was solved iteratively, using pivoting in order to invert the resulting difference matrix equations. Generally, 15–20 terms in the series were taken, with 701 mesh points. The accuracy of the calculations was seen to decrease with increasing Reynolds number $R_s$ and $\alpha$, although the results presented here appeared to be accurate to at least within 5 %. With increasing $R_s$ and $\alpha$ more under-relaxation was necessary, the old value of the $\Psi_m$ being updated by as little as 1 % of the calculated value in the most critical of the cases attempted.

One of the most noticeable features of the results is the region of separated flow which grows with increasing $R_s$. The separating streamlines for $\alpha = 10$ and $R_s = 50$, 70 and 90 are shown in figure 2. In figure 3 the variation with Reynolds number of the shear stress on the outer cylinder is plotted in the scaled form $\tau = \psi_{10\rho\rho}^{(s)}(\rho = \alpha)/R_s^{\frac{1}{2}}$

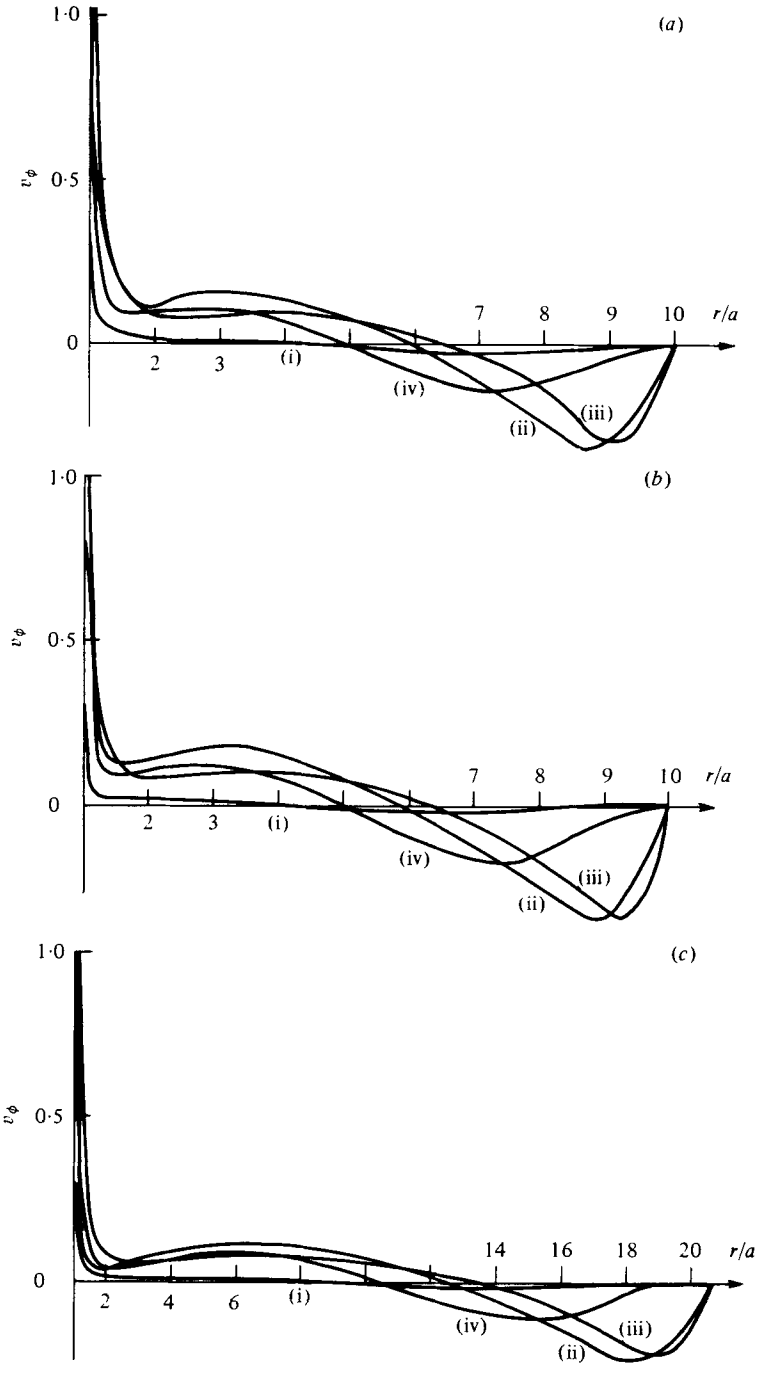


FIGURE 4. Graphs of the velocity component $v_\phi$ against radial distance $r/a$ for (*a*) $R_s = 50$, $\alpha = 10$, (*b*) $R_s = 90$, $\alpha = 10$ and (*c*) $R_s = 50$, $\alpha = 20{\cdot}67$. (i) $\phi = \frac{1}{2}\pi - 0{\cdot}1$, (ii) $\phi = \frac{1}{2}\pi - 1$, (iii) $\phi = \frac{1}{2}\pi - 1{\cdot}3$, (iv) $\phi = \frac{1}{2}\pi - 0{\cdot}5$.

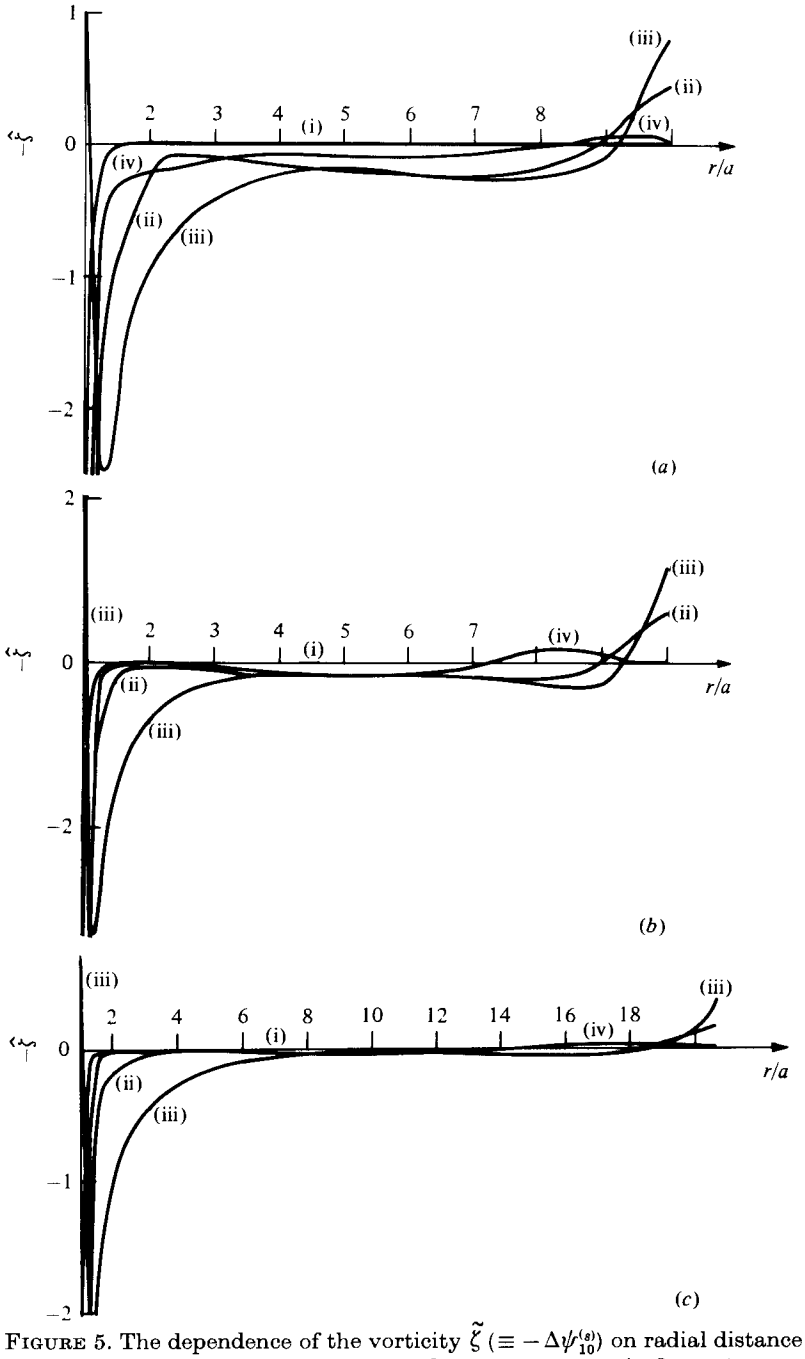


FIGURE 5. The dependence of the vorticity $\tilde{\xi}$ ($\equiv -\Delta\psi_{10}^{(s)}$) on radial distance $r/a$. (*a*)–(*c*) and (i)–(iv) correspond to same cases as in figure 4.

against $\phi$, as suggested by boundary-layer theory. The three sets (ii)–(iv) for $\alpha = 10$ show quite good correlation in figure 3, despite the likelihood of appreciable changes in the structure with varying Reynolds number because of the flow separation from the outer wall. Figures 4 (*a*)–(*c*) show the distribution of tangential velocity $v_\phi$ for $\alpha = 10$ with $R_s = 50$, for $\alpha = 10$ with $R_s = 90$ and for $\alpha = 20{\cdot}67$ with $R_s = 50$, respectively.

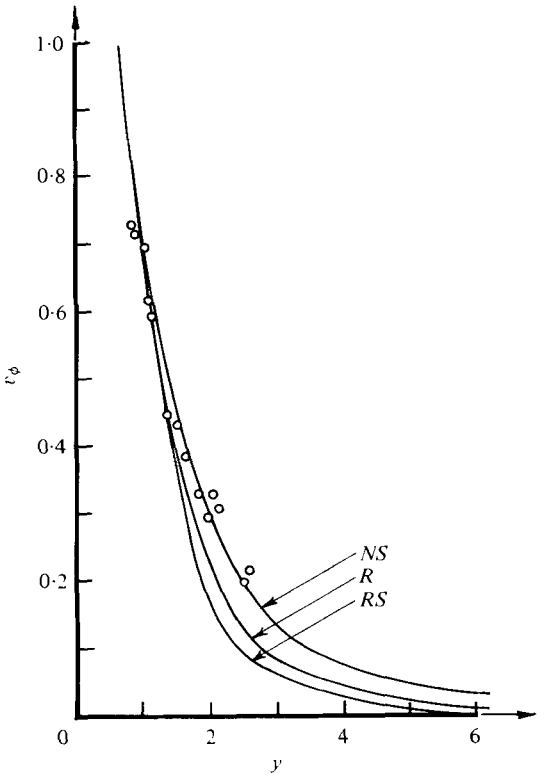


FIGURE 6. Comparison between the present solutions (*NS*) and Bertelsen's (1974) experimental results (circles) for the velocity $v_\phi$ *vs.* $y$ when $R_s = 90$, $\alpha = 20{\cdot}67$ and $\phi = \frac{1}{2}\pi - 1$. Also shown are the solutions of Stuart (1966) and Riley (1965) (*RS*) and of Riley (1975) (*R*) for the one-cylinder problem.

We note in passing that these solutions have not been corrected for Stokes drift or for the transformation correction. However, outside the Stokes layer, the Stokes drift is of course negligible and it is a simple matter to transform the $O(\epsilon)$ steady-streaming results from the $\zeta$ plane to the physical ($z$) plane.† All three sets of results exhibit similar characteristics for $v_\phi$. As the distance from the inner cylinder increases the velocity initially falls and reaches a positive plateau value; it then drops again to become negative, before returning to order $\alpha^{-5}$ on the outer cylinder. Figures 5(*a*)–(*c*) show the corresponding vorticity distributions. Comparison of the solutions for $\alpha = 10$ when $R_s = 50$ and $R_s = 90$ indicates that the core is becoming a region of constant vorticity as $R_s \to \infty$ (Batchelor 1956), with the streamlines in the core flow becoming closed.

Next we compare our solution of the full Navier–Stokes equations with the experimental results of Bertelsen for the case $\alpha = 20{\cdot}67$, $R_s = 90$. The comparison is shown in figure 6, where the tangential velocity at $\phi = \frac{1}{2}\pi - 1$ is presented and Bertelsen's (1974) normalization is used. The solution of the full equations of motion reproduces the experimental results to almost graphical accuracy, and in particular predicts a

† A referee has kindly pointed out that the transformation from the $\zeta$ to the $z$ plane is more complicated within the Stokes layer, however.

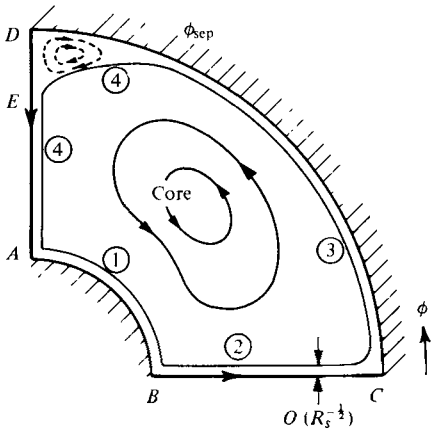


FIGURE 7. Sketch of the (core/boundary-layer) flow structure when $R_s \gg 1$ and $\alpha = O(1)$, including the separation at $\phi = \phi_{sep}$ on the outer cylinder.

residual outer slip at the edge of the Reynolds boundary layer (the boundary layer associated with the steady-streaming Reynolds number $R_s$ when $R_s \gg 1$).

For a fixed value of $\alpha$, therefore, the numerical flow solutions as $R_s$ increases vary with $R_s$ according to the orders of magnitude associated with classical boundary-layer theory, while the core vorticity tends to a uniform value. A sketch of the general large-$R_s$ flow is shown in figure 7. When $R_s \gg 1$ [but $\alpha$ is $O(1)$] the $O(R_s^{-\frac{1}{2}})$ boundary layer ① on the inner cylinder is driven [both by the inner-wall slip (3.29) and the core slip velocity] towards the equator, where it forces a free shear layer ② (see Davidson & Riley 1972; Smith & Duck 1977) towards the outer cylinder. The shear layer then attaches to the outer cylinder and forces a boundary layer ③ away from the equator. This boundary layer is driven by the core slip velocity and the outer-wall slip (3.30), but to avoid deceleration (and hence a catastrophic separation; Stewartson 1970) near the pole, it separates before reaching the pole, the separation (at $\phi = \phi_{sep}$ in figure 7) presumably being of the triple-deck, free-streamline, kind (Sychev 1972; Smith 1977). The shear layer ④ formed beyond separation constitutes part of the boundary for the core of uniform vorticity and (after the collision at the point $E$ in figure 7) it supplements the original boundary layer ① on the inner cylinder by attaching at that cylinder's pole (see figure 7). Following Stewartson (1958) and Lyne (1971), we assume that the velocity profiles at the ends of each boundary layer are convected around corners essentially unchanged. Smith & Duck's (1977) analysis of the end $B$ confirms that this approximation is fairly satisfactory. In all layers ①–④, $\psi_{10}^{(s)}$ and the transverse co-ordinate $n$ are both $O(R_s^{-\frac{1}{2}})$ [$\psi_{10}^{(s)} = R_s^{-\frac{1}{2}}\hat{\Psi}$ and $n = R_s^{-\frac{1}{2}}y$, say], so that the streamwise velocity $\partial\psi_{10}^{(s)}/\partial n$ is $O(1)$. The typical slip velocity of the core is also $O(1)$. So the layers ①–④ are all controlled by the classical boundary-layer equations (we let $x$ denote streamwise distance in each case) and have to match to the core slip velocity at their outer edges. The other boundary conditions are the wall slips (3.29)–(3.31) in ① and ③, a symmetry condition in ② and a zero-velocity condition in ④ [at least, until layer ④ collides with the line of symmetry $\theta = \frac{1}{2}\pi$ at $E$ (figure 7), after which a symmetry condition becomes appropriate on $EA$; the collision at $E$ is a form of reattachment and the flow details near such a reattachment are as yet unknown]. Between layer ④ and the outer cylinder it is assumed that a relative slow eddying flow takes

place, implying that, between separation and the point $E$, ④ acts as a free streamline (of constant pressure) for the inviscid core. This assumption is consistent with the triple-deck separation of ③ (see Sychev 1972; Smith 1977) and seems in keeping with our numerical solutions (figures 2 and 3).

The above, separated-flow description for $R_s \gg 1$ with $\alpha = O(1)$ agrees quantitatively with our Navier–Stokes solutions (figures 2–5), which in turn agree well with Bertelsen's (1974) experimental observations (figure 6). We consider next (§ 5) the properties of the above separated-flow description when $\alpha$ (as well as $R_s$) is large.

## 5. The flow model for large values of $\alpha$ and $R_s$

Suppose then that, in the large-$R_s$ flow description at the end of § 4, $\alpha$ is large, i.e. that the radius of the outer cylinder is much larger than that of the inner (Bertelsen (1974) has $\alpha = 13{\cdot}03$ and $20{\cdot}67$). When $\alpha \gg 1$ the boundary-layer motion acquires two distinct length scales, in both the $x$ and the $y$ direction, as depicted in figure 8. Further, we may ignore hereafter the slip on the other cylinder, since it is only $O(\alpha^{-5})$.

We postulate now that the velocities in the viscous layers ②–④ and in the inviscid core solution outside are an order lower in $\alpha^{-1}$ than the maximum velocities in the boundary layer ①. Hence the majority of ① has a jet-like form. So, after the collision at the equator $B$, a free jet is generated [when $x$ is $O(1)$] and asymptotes to the similarity form of Bickley (1937) on an $x$ scale $\gg 1$ (cf. Davidson & Riley 1972) but $\ll \alpha$. Then, because in the Bickley solution the jet thickness grows like $x^{\frac{2}{3}}$ while its velocity decays like $x^{-\frac{1}{3}}$, the velocities along most of ② (and hence ③ and ④) are $O(\alpha^{-\frac{1}{3}})$ only, but with a typical transverse ($y$) scale $O(\alpha^{\frac{2}{3}})$ [since, also, $x$ is $O(\alpha)$ in ②, ③ and ④]. Consequently, we split ① into two parts I and II (see figure 8) wherein $y \sim 1$ and $Y \sim 1$ respectively (here $Y = \alpha^{-\frac{2}{3}}y$). Further, we expand the stream function in the two parts as follows:

$$\left.\begin{aligned} \hat{\Psi}^{\mathrm{I}} &= \bar{\Psi}^{\mathrm{I}}_0(x,y) + \alpha^{-\frac{1}{3}}\hat{\Psi}^{\mathrm{I}}_1(x,y) + \ldots, \\ \hat{\Psi}^{\mathrm{II}} &= \alpha^{\frac{1}{3}}\Psi^{\mathrm{II}}_0(Y) + \Psi^{\mathrm{II}}_1(X,Y) + \ldots, \end{aligned}\right\} \tag{5.1}$$

where $x = \alpha X$. The main term in I, $\bar{\Psi}^{\mathrm{I}}_0(x,y)$, is precisely that discussed by Stuart (1966) and Riley (1965) and is the solution of the boundary-layer problem for a single cylinder:

$$\left.\begin{gathered} \hat{\Psi}^{\mathrm{I}}_{0y}\hat{\Psi}^{\mathrm{I}}_{0xy} - \hat{\Psi}^{\mathrm{I}}_{0x}\hat{\Psi}^{\mathrm{I}}_{0yy} = \hat{\Psi}^{\mathrm{I}}_{0yyy}, \\ \hat{\Psi}^{\mathrm{I}}_0(x,0) = \hat{\Psi}^{\mathrm{I}}_{0y}(x,\infty) = \hat{\Psi}^{\mathrm{I}}(0,y) = 0, \\ \hat{\Psi}^{\mathrm{I}}_{0y}(x,0) = \tfrac{3}{2}\sin 2x. \end{gathered}\right\} \tag{5.2}$$

It can be shown that, for $x$ small,

$$\hat{\Psi}^{\mathrm{I}}_0(x,y) = 3^{\frac{1}{2}}x[1 - \exp(-3^{\frac{1}{2}}y)] + O(x^3). \tag{5.3}$$

To detail the effects of finiteness of the domain we also need the next-order term in I, which satisfies

$$\left.\begin{gathered} \hat{\Psi}^{\mathrm{I}}_{0y}\hat{\Psi}^{\mathrm{I}}_{1xy} + \hat{\Psi}^{\mathrm{I}}_{1y}\hat{\Psi}^{\mathrm{I}}_{0xy} - \hat{\Psi}^{\mathrm{I}}_{0x}\hat{\Psi}^{\mathrm{I}}_{1yy} - \hat{\Psi}^{\mathrm{I}}_{1x}\hat{\Psi}^{\mathrm{I}}_{0yy} = \hat{\Psi}^{\mathrm{I}}_{1yyy}, \\ \hat{\Psi}^{\mathrm{I}}_1(x,0) = \hat{\Psi}^{\mathrm{I}}_{1y}(x,0) = 0, \\ \hat{\Psi}^{\mathrm{I}}_{1y}(x,\infty) = K \quad \text{(constant)}, \\ \hat{\Psi}^{\mathrm{I}}_1(x,y) = \Lambda(y) + O(x^2) \quad \text{for } x \text{ small}, \end{gathered}\right\} \tag{5.4}$$

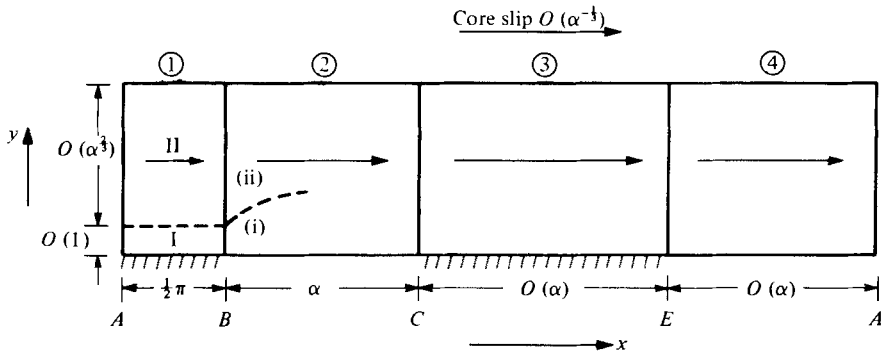


FIGURE 8. The structure of the boundary-layer flows ①–④ when $\alpha$ is large, according to § 5.

where

$$\Lambda(y) = 3^{\frac{1}{2}}Ky[\exp(-3^{\frac{1}{2}}y)+1]+\tfrac{1}{4}K\exp(-2\times 3^{\frac{1}{2}}y)+\sum_{n=3}^{\infty} C_n\exp(-3^{\frac{1}{2}}ny)$$
$$+(\tfrac{3}{2}K-\lambda_2)\exp(-3^{\frac{1}{2}}y)+\lambda_2-\lambda_1-\tfrac{7}{4}K, \quad (5.5)$$

$$C_n = -C_{n-1}(n-2)/n^2 \quad (n\geqslant 3), \quad C_2 = \tfrac{1}{4}K, \quad \lambda_1 = \sum_{n=3}^{\infty} C_n, \quad \lambda_2 = \sum_{n=3}^{\infty} nC_n. \quad (5.6)$$

The unknown constant $K$ here is due to the slip of the main profile $\Psi_0^{\mathrm{II}\prime}(Y)$ in II as $Y\to 0$:

$$\Psi_0^{\mathrm{II}}(Y) = KY+O(Y^3) \quad \text{as} \quad Y\to 0. \quad (5.7)$$

The motion in the outer part II remains independent of $x$ to first order because the typical streamwise length scale associated with the profile $\Psi_0'(Y)$ is $O(\alpha)$, not $O(1)$ (see below). We therefore suggest that the slip at the edge of the $O(R_s^{-\frac{1}{2}})$ boundary layer I, as observed by Bertelsen (1974), is due to the different length scales arising when $\alpha\gg 1$, for which the boundary layer ② spreads out to a thickness $O(\alpha^{\frac{2}{3}})$ (in order to accommodate the Bickley jet from $B$) and returns, via ④, as a much slower, but thicker layer.

The constant $K$ is determined by the longer-scale flow in ②–④ on the scale $X\sim 1$ and by the inviscid core, without direct recourse to ①. Since, in ②–④, $X$ and $Y$ (rather than $x$ and $y$) are $O(1)$, while the expansions (implied by the Bickley jet form) for $\hat{\Psi}$ and the corresponding streamwise velocity $\hat{u}$ are

$$\left.\begin{aligned}\hat{\Psi} &= \alpha^{\frac{1}{3}}\hat{\Psi}_0(X,Y)+O(1),\\ \hat{u} &= \alpha^{-\frac{1}{3}}\hat{u}_0(X,Y)+O(\alpha^{-\frac{2}{3}}),\end{aligned}\right\} \quad (5.8)$$

the governing equations for $\hat{\Psi}_0(X,Y)$ and $\hat{u}_0(X,Y)$ in layers ②–④ remain the classical boundary-layer equations. The matching conditions at the edges of ②–④ join the flow to the slipping motion of the inviscid core, wherein

$$\psi_{10}^{(s)} = \alpha^{\frac{2}{3}}\psi_c(\rho/\alpha,\phi)+O(\alpha^{\frac{1}{3}}), \quad \Delta\psi_c = -\omega_c \quad \text{(constant)} \quad (5.9)$$

because the slip velocity is $O(\alpha^{-\frac{1}{3}})$ from (5.8). The inner conditions on ②–④ require symmetry along ②, no slip along ③ and zero velocity along ④ (except on $EA$, where symmetry is required). Figure 8 is a sketch of the large-$\alpha$ boundary-layer flow structure.

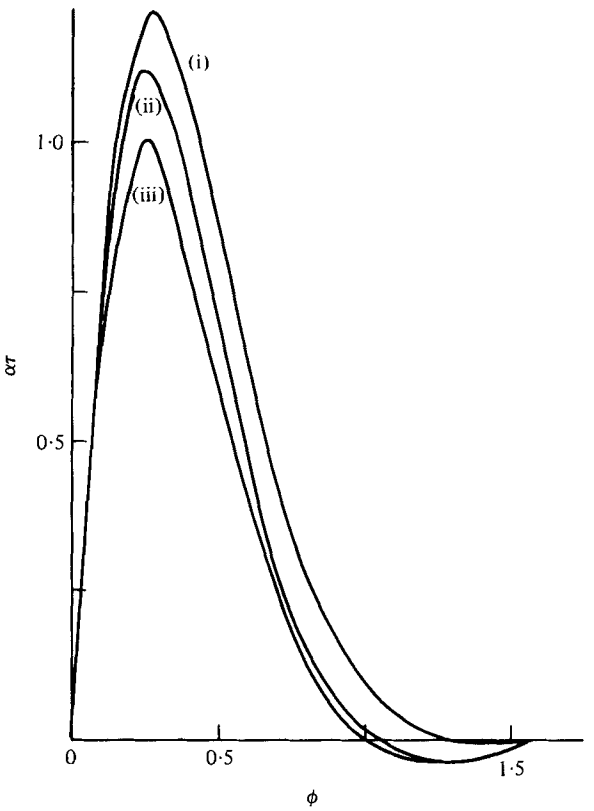


FIGURE 9. Graphs of $\alpha$ times the effective shear stress $\tau$ (on the outer cylinder) against $\phi$ for (i) $R_s = 50$, $\alpha = 5$, (ii) $R_s = 50$, $\alpha = 10$ and (iii) $R_s = 50$, $\alpha = 20{\cdot}67$.

The cause of this longer-scale behaviour is the starting form of layer ②, which has a double structure [(i) and (ii) below] for $X$ small, reminiscent of the Goldstein (1930) wake.

In (i), where $Y \sim X^{\frac{2}{3}}$,

$$\hat{\Psi}_0 = X^{\frac{1}{3}} g_0(\eta) + O(X^{\frac{2}{3}}), \tag{5.10}$$

where $\eta = Y/X^{\frac{2}{3}}$. Here $g_0(\eta)$ is the Bickley jet solution, i.e.

$$\left.\begin{aligned} g_0(\eta) &= (\tfrac{9}{2}N)^{\frac{1}{3}} \tanh \tilde{\eta} \\ \text{where} \qquad \tilde{\eta} &= (\tfrac{1}{48}N)^{\frac{1}{3}} \eta \end{aligned}\right\} \tag{5.11}$$

and $N$ is the momentum flux in the jet. This starting form matches the finite-scale ($x$) solution in ① with the long-scale ($X$) solution in ②. Thus effectively the Bickley jet is buried within the thicker classical boundary layers ②–④ when $\alpha$ is large, even though in a sense the Bickley jet is itself responsible for setting up the flows in ②–④.

In (ii), where $Y \sim 1$,

$$\hat{\Psi}_0 = \Psi_0(Y) + X^{\frac{1}{3}} \Phi_1(Y) + O(X^{\frac{2}{3}}) \quad \text{for} \quad X \ll 1, \tag{5.12}$$

where $\Psi_0(Y)$ is the terminal profile of ④, in (5.1) and (5.7). Hence the inner cylinder plays the role of a point source of momentum, generating a free shear layer in ②, a boundary layer in ③ and another free shear layer in ④. The $x$-scale and $X$-scale

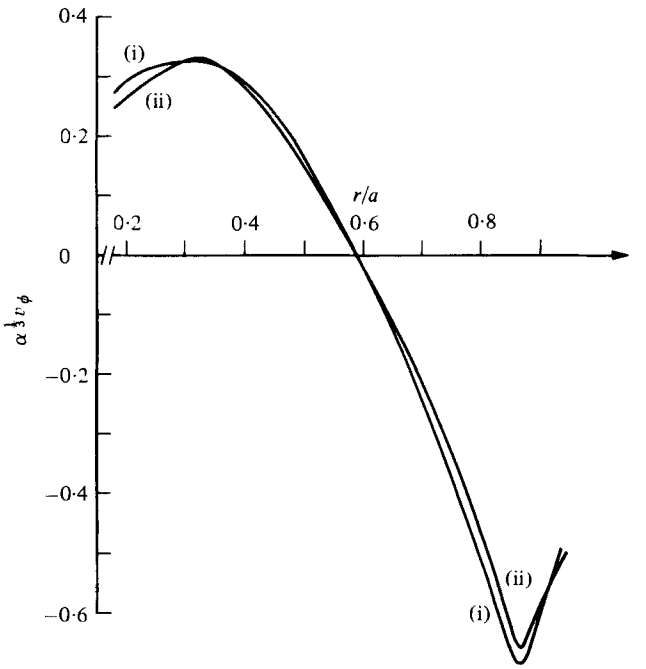


FIGURE 10. Graphs of $\alpha^{\frac{1}{3}}$ times the core velocity $v_\phi$ against $r/a$ for (i) $R_s = 50$, $\alpha = 10$ and (ii) $R_s = 50$, $\alpha = 20{\cdot}67$. Here $\phi = \frac{1}{2}\pi - 1$.

motions match via (5.10)–(5.12) and because the shear layer in ④ feeds into the outer part II of the boundary layer ① and so sweeps almost unaltered past the inner cylinder. It then completes the circuit by joining into ②, through the outer zone (ii) of (5.12) (see figure 8).

The (small) core vorticity [$\alpha^{-\frac{1}{3}}\omega_c$, from (5.9)] is fixed by the condition of periodicity. Once $\omega_c$ and hence the layers ②–④ have been determined, the constant $K$, which gives the residual slip at the edge of part I of the inner cylinder's boundary layer, follows from (5.7). We have not attempted to solve the large-$\alpha$ problem of layers ②–④ with the inviscid core, because the separation of ③ and the unknown position of ④ introduce extreme difficulties. However, the predictions of this large-$\alpha$ theory are found to be very much in line with the trends of the Navier–Stokes solutions of § 4 as $\alpha$ increases there. Thus the $\alpha^{-1}$ variation [proposed by (5.8)] in the effective ($R_s$-scaled) wall shear $\tau = [\partial\hat{u}/\partial y]_{y=0}$ on the outer cylinder seems to be well borne out in figure 9, where graphs of $\alpha$ times the effective wall shear $\tau$ of figure 3 are presented. The numerical solutions appear to approach a limit as suggested. Also, as is shown in figure 10, where the results for $\alpha = 10$, 20·67 and $R_s = 50$ are shown in rescaled form, the full Navier–Stokes solutions do seem to produce the $O(\alpha^{-\frac{1}{3}})$ velocity in the inviscid core, as predicted by the asymptotic theory (5.9).

## 6. Conclusion

We believe that the Navier–Stokes solutions of § 4 have demonstrated the importance of the outer cylinder in the two-cylinder problem, resolving (see figure 6) the discrepancy between the experimental results of Bertelsen (1974) and previous (one-cylinder)

theories. The solutions of the full Navier–Stokes equations also appear to agree remarkably well with the asymptotic theory (§ 5) for $\alpha \gg 1$, especially when one considers that the values of $\alpha^{-\frac{1}{3}}$ in the examples computed were fairly large

$$(10^{-\frac{1}{3}} \doteqdot 0{\cdot}459, \quad (20{\cdot}87)^{-\frac{1}{3}} \doteqdot 0{\cdot}365)$$

whereas the asymptotic theory required $\alpha^{-\frac{1}{3}} \ll 1$. Indeed, it is the fact that the influence of the outer cylinder decays only as $\alpha^{-\frac{1}{3}}$ that makes the outer-cylinder effect so significant even when $\alpha$ is large. On the other hand, although the problem for calculating the slip constant $K$ when $\alpha \gg 1$ has been posed (§ 5), the numerical work involved in such a calculation is formidable. The main difficulty concerns the unknown position of the separating streamline from the outer cylinder (see figures 2 and 7). However, the expansions given in § 5 are believed to provide a self-consistent account of the overall motion when $\alpha$ is large, and the tests in figures 9 and 10 support this view.

The authors wish to thank Professor J. T. Stuart for many helpful discussions concerning this work, and the referees for pointing out errors in an earlier version of this paper. One of us (PWD) acknowledges the receipt of an S.R.C. post-doctoral research grant.

## REFERENCES

Batchelor, G. K. 1956 *J. Fluid Mech.* **1**, 177.
Bertelsen, A. F. 1974 *J. Fluid Mech.* **64**, 589.
Bertelsen, A. F., Svardal, A. & Tjøtta, S. 1973 *J. Fluid Mech.* **59**, 493.
Bickley, W. G. 1937 *Phil. Mag.* **23**, 727.
Davidson, B. J. & Riley, N. 1972 *J. Fluid Mech.* **53**, 287.
Goldstein, S. 1930 *Proc. Camb. Phil. Soc.* **26**, 1.
Holtsmark, J., Johnsen, I., Sikkeland, T. & Skavlem, S. 1954 *J. Acoust. Soc. Am.* **26**, 26.
Lyne, W. H. 1971 *J. Fluid Mech.* **45**, 13.
McConalogue, D. J. & Srivastava, R. S. 1968 *Proc. Roy. Soc.* A **307**, 37.
Riley, N. 1965 *Mathematika* **12**, 161.
Riley, N. 1967 *J. Inst. Math. Appl.* **3**, 419.
Riley, N. 1975 *J. Fluid Mech.* **68**, 801.
Segel, L. A. 1961 *Quart. Appl. Math.* **18**, 335.
Skavlem, S. & Tjøtta, S. 1955 *J. Acoust. Soc. Am.* **27**, 26.
Smith, F. T. 1974 *J. Inst. Math. Appl.* **13**, 127.
Smith, F. T. 1977 *Proc. Roy. Soc.* A **356**, 443.
Smith, F. T. & Duck, P. W. 1977 *Quart. J. Mech. Appl. Math.* **30**, 143.
Stewartson, K. 1958 *Proc. Symp. P.L. Res. Freiburg i. Br.*, 1957, pp. 57–91. Springer.
Stewartson, K. 1970 *J. Fluid Mech.* **44**, 347.
Stuart, J. T. 1963 In *Laminar Boundary Layers*, chap. 7. Oxford University Press.
Stuart, J. T. 1966 *J. Fluid Mech.* **24**, 673.
Sychev, V. Ya. 1972 *Izv. Akad. Nauk SSSR, Mekh. Zh. Gaza* **3**, 47.
Wang, C. Y. 1968 *J. Fluid Mech.* **32**, 55.